Slowing Down DNA Translocation through Solid-State Nanopores by Edge-Field Leakage

Ceming Wang
University of Notre Dame https://orcid.org/0000-0002-1328-6410
Sebastian Sensale
University of Notre Dame
Zehao Pan
University of Notre Dame
Satyajyoti Senapati
University of Notre Dame
Hsueh-Chia Chang (hchang@nd.edu)
University of Notre Dame

Article

Keywords: solid-state nanopores, DNA translocation, electric field leakage

Posted Date: July 28th, 2020

DOI: https://doi.org/10.21203/rs.3.rs-45233/v1

Version of Record: A version of this preprint was published at Nature Communications on January 8th, 2021. See the published version at https://doi.org/10.1038/s41467-020-20409-4.

Slowing Down DNA Translocation through Solid-State Nanopores by Edge-Field Leakage

Ceming Wang[1], Sebastian Sensale[2], Zehao Pan[1], Satyajyoti Senapati[1] and Hsueh-Chia Chang[1, 2]*

[1] *Department of Chemical and Biomolecular Engineering, University of Notre Dame, USA*

[2] *Department of Aerospace and Mechanical Engineering, University of Notre Dame, USA*

* *e-mail: hchang@nd.edu*

Solid-state nanopores allow high-throughput single-molecule detection but identifying and even registering all translocating small molecules remain key challenges due to their high translocation speeds. We show here the same electric field that drives the molecules into the pore can selectively pin and delay their transport. A thin high-permittivity dielectric coating on slender bullet-shaped polymer nanopores permits electric field leakage at the pore tip to produce a voltage-dependent surface field on the upper periphery of the pore that can reversibly edge-pin entering molecules that can absorb conformally to the tip corner. This localized tip field renders molecular entry an activated process with sensitive exponential dependence on the bias voltage and molecular rigidity. The exponential sensitivity allows us to selectively prolong the translocation time of short single-stranded DNA molecules by up to 5 orders of magnitude, allowing discrimination against their double-stranded duplexes with 97% confidence. We show evidence that the leak-field pinned single-stranded DNA actually absorbs onto the edge before entering the pore, yielding translocation times as long as minutes.

Solid-state and protein nanopores are an emerging class of single-molecule sensors for DNA sequencing[1–3], protein detection[1,4,5], and DNA-protein complex analyses[6]. The Achilles heel of nanopores has been the inability to control the motion of biomolecules during voltage-driven translocation through the pore[1,3,7–9]. With the development of enzyme-based methods that ratchet polynucleotides through the pore, the first nanopore-sequencer has been realized using protein nanopores[3]. Despite the progress that has been made with biological nanopores, solid-state nanopores with high stability and tunable pore diameters still offer several advantages. They facilitate integration with compact electronic/optical sensor modalities and allow higher throughput than their protein counterparts. However, developing solid-state nanopore sensors capable of complete characterization of the translocating biomolecules has been challenging[1,7,9], primarily because of the fast electrophoretic translocation by highly focused electric fields at the pore. The high fields are due to the nanoscale pore dimensions necessary for resistive current signals above thermal noise, and the minimum bias voltage (20-60 mV)[10] necessary to overcome barriers due to conformation entropy, electrostatic repulsion, and electro-osmotic flow[11,12].

Typical electrophoretic velocities of nucleic acids across solid-state nanopores are 10-1000 ns per base[1]. At these high velocities, short nucleic acids (<100 nt) as well as small protein molecules are often undetected, much less identified[13]. Thus, a high signal bandwidth (> 1 MHz) is needed to fully resolve the resistive pulses[14,15]. High signal bandwidth, however, also strongly amplifies thermal noise in the current recordings; this noise makes the signal resistive pulses become undetectable[16]. This limitation hence prevents accurate profiling of promising cancer biomarkers like proteins, short mRNA fragments, and microRNAs (19-22 nt) by solid-state nanopores[13,17,18]. For the proposed sequencing applications by quantum tunneling, speed control is also a key issue for realizing practical

quantum sequencers[9]. An additional mechanism to dramatically reduce (by orders of magnitude) and control the fast electrophoretic velocity of molecules is therefore necessary to realize sensitive and selective solid-state nanopore sensors for short nucleic acids and other small biomolecules[13] and sequencing platforms[2,19].

Multiple approaches have been proposed to slow down the translocation events[20], which involve either modifying the properties (mostly viscosity) of the electrolyte[10,21,22], incorporating optical (or magnetic) traps or tweezers[20,23,24], or using protein tags to slow down the motion of the smaller molecules[25–27]. In the last few years, surface charge density modulation has also been suggested to slow down translocation events[28–33], mostly by building nanopores with dielectric materials like Al_2O_3[29,32,34,35] and HfO_2[30], or by exploring optoelectronic control of surface charge[33]. However, these modifications produce a gating field that is much weaker than the driving field along the pore and are only capable of reducing the translocation speed by at most one order of magnitude[29,30,33,35], which is small compared to the typical two-decade wide bandwidth of the Poisson distribution of translocation times. Interference with the sensing current signals is also a problem[9].

In this article we will show that the deposition of a high-permittivity Al_2O_3 film over an insulating bullet-shaped polymer nanopore allows the field to leak through the dielectric material and into the upper membrane, producing a field comparable in intensity to the translocation field yet sufficiently weak to prevent permanent trapping of the molecules (and clogging of the nanopores). By properly tuning the bullet-shaped geometry, which has a conical base and a short straight pore at the tip, this field can induce a net voltage-dependent surface charge density on the upper membrane, which can reversibly edge-pin flexible translocating molecules, rendering molecular entry into the pore an activated process. The translocation time becomes a strong function of the molecular rigidity, which is ideally suited for discriminating between short (< 100 nt) single-stranded and duplex nucleic acids whose persistence length differ by two orders of magnitude. We can selectively prolong the translocation time of short single-stranded DNA molecules by 5 orders of magnitude, thus allowing discrimination against their double-stranded duplexes with 97% confidence. Since the leakage field is outside the nanopore, it does not interfere with the resistive signal current from within the pore tip.

Electric Field Leakage through Dielectric Materials

Ideal dielectrics are assumed to be perfect insulators[36] (that is, they present infinite resistivity). However, in reality, their resistivity is finite, leading to a passage of current when subjected to applied voltages commonly known as current leakage[36,37]. This leakage is often undesirable, as it decreases the effective electric field needed for the functioning of multiple devices and promotes material degradation processes[37–39]. In materials often used in nanopores, such as SiO_2, Si_3N_4 and Al_2O_3, this leakage is often associated with Poole-Frenkel effects[36,40] and it manifests at voltages of the order of 10^8 V/m[41]. There is no significant current leakage at lower electric fields. However, due to the finite permittivity of these material, field lines can penetrate the dielectric film leading to significant field leakage[42,43].

Optical and electric intensity can become singular at metallic or dielectric cones or wedges. These singular fields are present in tip plasmonics[44], knife-edge scattering[45], Taylor cones of electrified drops[46], etc. In our earlier microchannel electro-osmosis work, the singular tangential electric field at a 90-degree turn of an insulating wall was converted into a comparably singular leakage field across the corner by introducing finite wall permittivity[42,43]. The leakage field exits the other side of the corner as an intense normal field that can arrest the transport of micro-colloids and trap them at the upstream side of the corner. This same mechanism can be incorporated into nanopore devices, leading to high electric fields normal to the upper membrane of the nanopore which are capable to pin the molecules to the tip of the nanopore.

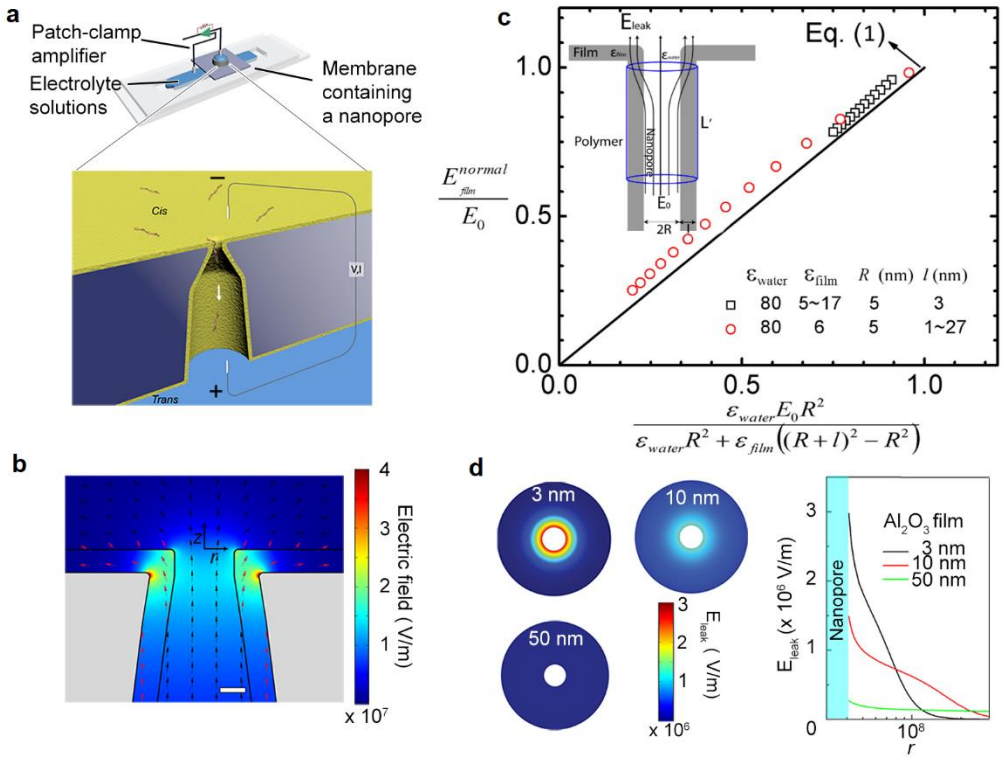

Figure 1. **The electric field leakage effect in Al_2O_3-coated polymer nanopores. a.** Set-up to measure resistive pulses from the translocation of individual DNA molecules through single bullet-shaped polymer nanopore coated with a thin Al_2O_3 layer. **b.** Electrostatic modelling of a Al_2O_3-coated bullet-like nanopore (tip diameter: 8 nm, half cone angle: 8°) was simulated with an applied voltage of 0.5 V. Electric field lines and intensity evaluated numerically on the tip side of the Al_2O_3-coated polymer nanopore. The electric field is significantly enhanced and develops a normal field leakage near the sharp pore edge. Scale bar = 3 nm. **c**. Validation of Eq. (1) through the use of finite-element-method simulations for normal field leakage in the dielectric film. Different permittivities and film thicknesses were sampled. Inset shows the schematics of a high-permittivity dielectric film on an insulating polymer nanopore orifice and the Gauss volume used to estimate the leaked field around the pore. **d.** Left: Surface plots of the strength of normal leakage field (E_{leak}) showing the normal leakage field at the pore edge is a strong function of Al_2O_3 film thickness (nanopore diameter, 8 nm). Right: Axial dependence of the normal leakage field as a function of distance from the pore mouth r for three Al_2O_3 film thicknesses.

Our designed solid-state nanopore has a conical base and a short straight pore at the tip (see Fig. 1a and Supplementary Materials S4). The conical base with the insulating PET (Polyethylene terephthalate) membrane wall focuses the electric field and the high-permittivity Al_2O_3 film on the straight pore edge facilitates field leakage at the tip end (see Fig. 1b). Once the field lines enter the dielectric film inside the pore, the axially conditioned parallel field lines within the straight pore region ensure that the field intensity in the dielectric film is identical to that in the aqueous phase in the pore, despite the higher permittivity of the latter phase. With the converging geometry at the conical base, the field lines are confined to the aqueous bulk. A simple Gauss volume flux balance then allows us to relate the normal leakage field E_{leak} and the average electric field E_0 in the pore entrance at the neck with the conic base,

$$E_{leak} = E_{film}^{normal}\left(\frac{\varepsilon_{film}}{\varepsilon_{water}}\right) = \frac{E_0\varepsilon_{film}}{\varepsilon_{water} + \varepsilon_{film}((1 + l/R)^2 - 1)} \quad (1)$$

where ε_{water} and ε_{film} are the permittivity of water and dielectric film, respectively, R is the radius of nanopore orifice, and l is the thickness of the dielectric film (see Fig. 1c). E_{film}^{normal} is the field inside the dielectric membrane, which can be considered to be equal to the field in the liquid region E_{water}^{normal} (near the tip of the pore) for large pores and small values of l (see Supplementary Materials S1). Two limits of Eq. (1) are instructive. For l/R approaching infinity, corresponding to a non-polymeric dielectric membrane whose area is much larger than the pore tip area, E_{leak}/E_0 scales as $(R/l)^2 \ll$

1. This indicates conventional solid-state nanopores fabricated in dielectric membranes (such as SiN, SiO_2 and Al_2O_3 etc.) cannot produce significant molecule-pinning field at the pore edge, as the field is distributed over a large surface area that scales as l^2. Indeed, to date, there has been no experimental report of prolonging translocation times in dielectric membrane nanopores by edge field leakage. In fact, this field penetration across the entire dielectric membrane causes significant dielectric noise in the nanopores[14,47,48]. The other limit of l/R approaching zero yields that $E_{leak} \sim E_0(\varepsilon_{film}/\varepsilon_{water})$. The leakage field would then be proportional to the applied field and of comparable intensity if the permittivity ratio is not too small. Hence, a compound pore, with a nearly insulating polymer membrane and a thin high-permittivity dielectric film, is necessary for a leakage field with intensity and dimension that can delay the molecular translocation time without generating significant noise in the resistive signal. Finite-element-method simulations confirm that the electric field intensity within the dielectric film increases considerably and develops a normal field leakage when approaching the pore edge. In Fig. 1d, the intensity of normal leakage field along the r axis is shown for different film thicknesses l (3-50 nm). The rapidly increasing (singular) intensity of normal field at the pore edge with decreasing l confirms enhanced field leakage in PET nanopores coated with a thin Al_2O_3 film. Note that the zero-thickness limit is singular, as the field at the pore edge would be purely tangential for a perfectly insulating membrane.

To create our nanopores, we fabricate single nanopores with asymmetric shapes in PET membranes by the track-etching method[49] and subsequently deposit an Al_2O_3 dielectric film on the pore wall by Atomic Layer Deposition (ALD)[41,50]. The strength of the electric field at the pore tip can be fine-tuned through the choice of cone angles under the same applied voltage. The as-fabricated nanopores with large cone angles have a bullet-like shape while nanopores with small cone angles have a trumpet-like shape[51](Supplementary Materials S4). PET is highly insulating and has been used as supporting substrate to significantly reduce the dielectric noise of nanopores in dielectric membranes[48]. Al_2O_3 has a large dielectric constant of 8. ALD offers precise control of nanoscale film thickness. Details of the fabrication and characterization of Al_2O_3 PET nanopores have been described previously[50].

Field leakage induced delay of DNA translocation

Having fabricated the Al_2O_3-coated PET nanopores, we next tested the field leakage effect on the translocation of DNA molecules. We selected 22 nucleotides (nt) long single stranded DNA (ssDNA) molecules as representative small nucleic acid molecules whose fast translocation poses a major challenge to their detection by other solid-state nanopores[17]. Fig. 2a presents typical current traces recorded during the translocation of these molecules for a bare bullet-shaped PET nanopore without Al_2O_3 film coating and for one with a 3 nm Al_2O_3 film coating (diameter 10 nm). Resolvable signals due to translocation events are only observed in bullet nanopores coated with Al_2O_3 films, where substantial field leakage occurs. Moreover, the translocation time strongly depends on the Al_2O_3 film thickness. By comparing these two nanopores, we see an increase of one order of magnitude in the observed average translocation time, from 13 ms to 159 ms (see Fig. 2b), when the thickness of Al_2O_3 film decreases from 10 nm to 3 nm. As suggested from our field flux balance, the field leakage at the pore edge is indeed expected to become stronger with thinner Al_2O_3 dielectric layer. In contrast, no translocation event is detected for bare bullet PET nanopores without the high-permittivity dielectric layer that sustains field leakage—it is a singular limit. The correlation between dielectric film thickness and translocation time is observed in all tested Al_2O_3–coated PET nanopores at different bias voltages.

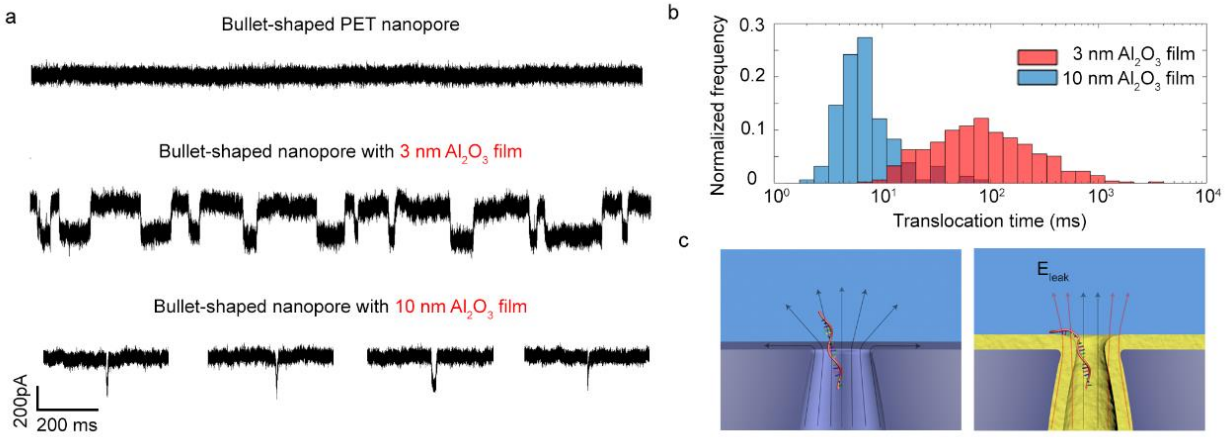

Figure 2. Slowing down ssDNA translocation speed with electric field leakage. a, Representative current traces for 22 nt ssDNA translocation through a bare bullet-shaped PET nanopore without Al_2O_3 film coating (diameter, 16 nm) and two bullet-shaped nanopores coated with 3 nm or 10 nm Al_2O_3 film under an applied voltage of 500 mV. Both Al_2O_3-coated nanopores have the same final tip diameter (10 nm). All three nanopores have similar bullet-like shapes (half cone angle ~ 7 ± 2°). Slow translocation of 22 nt ssDNA is observed using nanopores with thin Al_2O_3 film coating and the average translocation time is a function of film thickness. **b,** Normalized histogram of translocation times for nanopores with 3 nm or 10 nm Al_2O_3 film. Average translocation time: 3 nm Al_2O_3 film, 159 ms; 10 nm, 13 ms. **c,** Schematic showing the dominant tangential electric field at the bare PET nanopore edge results in a fast translocation of 22 nt ssDNA (left) while the normal leakage field at the Al_2O_3-coated nanopore edge traps the ssDNA and thus reduces its mobility.

Other than dielectric film thickness, different field leakage strengths can also be fine-tuned by varying cone angles of nanopore or bias voltages, as expected from Eq. (1). Previous studies have shown that the translocation of 100 nt ssDNA can be slowed down to ~ 0.18 ms using solid-state nanopores in Al_2O_3 membranes[29]. We observed an average translocation time ~ 125 ms for 22 nt ssDNA in Al_2O_3–coated PET nanopores (half cone angle ~ 9 ± 2°, diameter 8 nm, applied voltage 400mV). Due to confinement effects and electrostatic interactions, translocation times of DNA molecules (and other small molecules) through small-diameter (and/or charged) nanopores are well-modeled as activated processes[52–55]. As the electric field E_0 pulls the stalled DNA into the pore with a force qE_0, where q is the effective charge of the molecule, translocation times decrease exponentially with the field in such activated entries, reducing the barrier by a factor $\Delta G \sim \int_0^L qE_0 dz$ associated to the work done by the applied field to move the DNA molecule a distance L[53,54]. Translocation times can then be estimated through $\tau_0 e^{-\Delta G/k_B T}$, where τ_0 is the zero-field translocation time, k_B is Boltzmann constant, and T is the temperature of the system[52–54]. In contrast, larger diameter nanopores with small surface charge densities only weakly interact with the translocating molecule and thus they do not exhibit activation barriers, leading to translocation times inversely proportional to the external electric fields, as the electrostatic forces balance with hydrodynamic drag[56–58]. For our Al_2O_3–coated PET nanopores, when the applied voltage was slightly increased from 400 to 600 mV, the average translocation time increased five-fold, from 125 to 1217 ms (see Fig. 3), suggesting that field leakage increases the activation barrier, opposing translocation as illustrated in Fig. 2c.

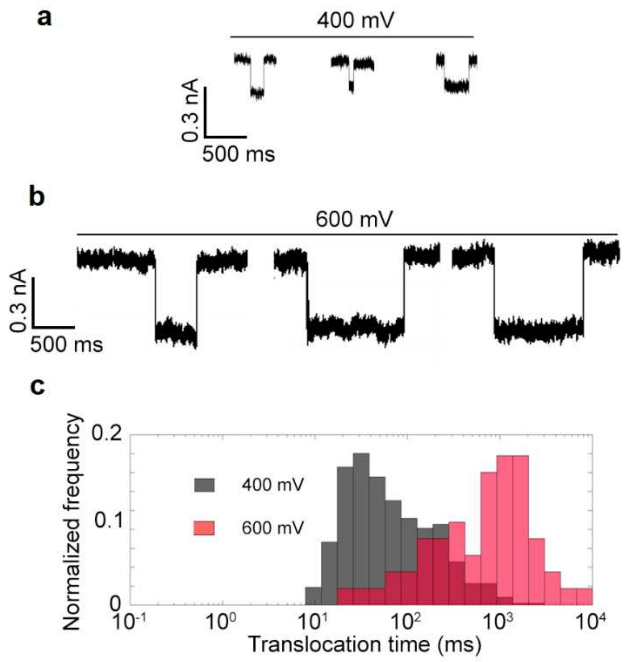

Figure 3. Effects of electric field leakage on ssDNA transport. a, Representative translocation signals for 22 nt ssDNA translocations at applied voltages of 400 mV. **b,** Representative translocation signals for 22 nt ssDNA translocations at applied voltages of 600 mV. **c,** Normalized histogram of corresponding translocation times at applied voltages of 400 mV and 600 mV and average translocation time as a function of applied voltage. Increasing the strength of electric field leakage can increase the translocation time of ssDNA. Data were acquired using a nanopore coated with 3 nm Al_2O_3 film (diameter, 8 nm; half cone angle, 9 ± 2°).

To realize the full potential of field leakage induced retardation of ssDNA, we investigated different geometries to enhance field leakage. We use a series of bullet Al_2O_3–coated nanopores (diameter, 10 nm) with different half cone angles at their conical base. Nanopores with larger half cone angles θ allow more electric field to be focused at the nanopore tip under the same applied voltage, as[50]

$$E_0 \sim \frac{V}{L'} + \frac{Vtg\theta}{R}, \quad (2)$$

with L' the length of the nanopore (11.5 μm in all our experiments). Therefore, larger half cone angles allow higher magnitude of normal field leakage, according to Eq. (1). Such asymmetric nanopores with different half cone angles were fabricated by varying etching times after breakthrough (see Supplementary Material S10). Fig. 4a compares four representative current traces through four Al_2O_3–coated nanopores with half cone angles ranging from 4° to 20°. The magnitude of corresponding electric field E_0 at the pore tip is indicated in Fig 4a, while translocation times are presented in Fig. 4c. Strikingly, with the increase of E_0 and thus normal leakage field, the average translocation time can be increased exponentially from tens of milliseconds to hundreds of seconds due to the activated nature of the entry.

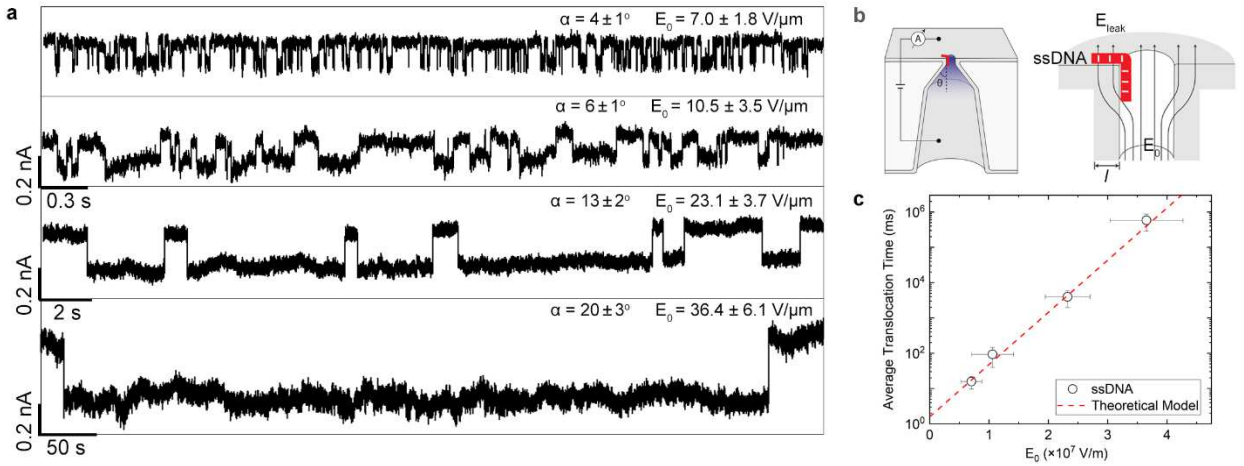

Figure 4. Modulation of translocation dynamics by angle control. a, Representative current traces of 22 nt ssDNA translocating through four bullet-shaped Al_2O_3–coated (thickness, 3 nm) nanopores (diameter, 10 nm) with different half cone angles (α). The nanopores with larger cone angle allow more electric field (E_0, as indicated) to be focused at the nanopore tip under the same applied voltage (500 mV) and thus higher magnitude of normal leakage field at the pore edge. With the increase of half cone angle and thus normal leakage field, the average translocation time can be increased exponentially from milliseconds to hundreds of seconds. **b,** Left: schematic of the measurement apparatus using a bullet-shaped Al_2O_3–coated nanopores with a half cone angles of θ. Right: zoom in of the nanopore orifice with ssDNA electrostatically trapped at the pore edge by the normal leakage field. **c,** The average translocation time dependence of E_0. The line represents the fit of the data to the theoretical model Eq. (4) with $\tau_0 = 1.595$ ms, a charge per nt of 0.1e, and a length per nucleotide of 0.64nm[59].

The high tunability of molecular pinning mechanism by varying the leakage field allows versatile control of translocation processes, which is difficult for other interactions[29]. It is expected that the charge, length, and mechanical properties of the translocating molecules can sensitively change the barrier and the translocation time, since the normal leakage field is confined to a film less than 3 nm in width. To test this selectivity, we analyzed translocation events of 22 base-pairs (bp) long double stranded DNA (dsDNA) molecules. The sample current traces for typical dsDNA translocation events and translocation time histograms at applied voltages of 400 mV and 600 mV are presented in Fig. 5. Interestingly, at both voltages, the translocation speed for dsDNA is observed to be orders of magnitude faster than that for the ssDNA. For example, at 400 mV, the average translocation time of dsDNA is around 4 ms, which is two orders of magnitude shorter than that of the ssDNA (and two orders of magnitude larger than reported translocation times in other nanopores[17,29]). The translocation time of dsDNA has an opposite voltage-dependence to the ssDNA. Increasing the applied voltages from 400mV to 600 mV, the translocation time of dsDNA decreases from 4 ms to 1.5 ms, suggesting that the normal leakage field has much less effect on dsDNA translocation than on its ssDNA counterpart. With the opposite trends of ssDNA and dsDNA translocation times on voltage bias, the mean translocation times of the two molecules are about a factor of ~ 811 different at 600 mV and, taking into account the spread in their distributions, the probability of a ssDNA exhibiting the same translocation time as a dsDNA is less than 3 % (Fig. 6a) . Since an excess of ssDNA molecules with long translocation times will increase the assay time for a given number of translocation events, the selectivity gained at high field comes with a trade-off in longer assay time for ssDNA-rich mixtures (see Supplementary Materials S8).

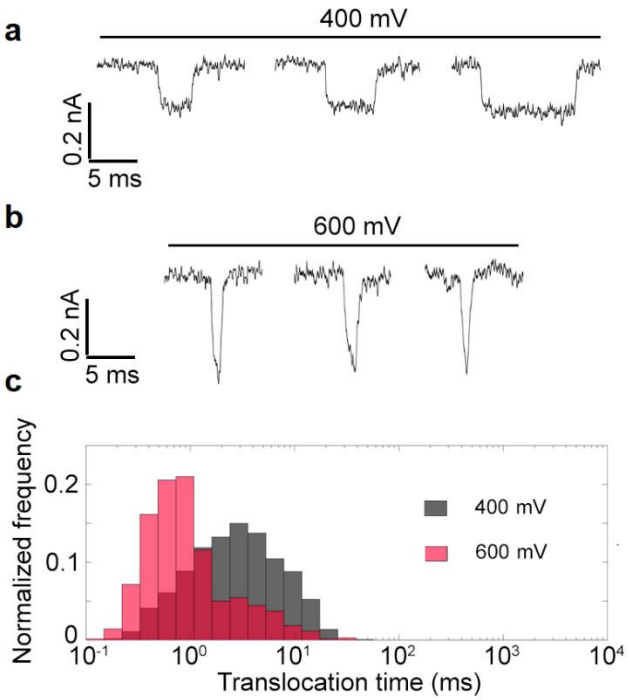

Figure 5. Effects of electric field leakage on dsDNA transport. a, Rrepresentative translocation signals for 22 bp dsDNA translocations at applied voltages of 400 mV. **b,** Rrepresentative translocation signals for 22 bp dsDNA translocations at applied voltages of 600 mV. **c,** Normalized histogram of corresponding translocation times at applied voltages of 400 mV and 600 mV and average translocation time as a function of applied voltage. Increasing the strength of electric field leakage decreases the translocation time of dsDNA. Data were acquired using a nanopore coated with 3 nm Al^2O^3 film (diameter, 8 nm; half cone angle, 9 ± 2°).

To explain these differences in translocation times, we may estimate the influence of field leakage on the activation barrier of the translocation events. When field leakage is involved, the driving field through the pore tip is reduced from E_0 to E_{water}^{normal}. Thus, there is a force qE_{water}^{normal} which pulls the molecule into the pore, and one qE_{leak} that opposes it (see Fig. 3c). Assuming field leakage to be uniform for all base pairs outside the pore (and not to affect the bases inside it), these forces may be integrated from $z = 0$ (all bps outside) to $z = L$ (all bps inside), leading to an estimate of the barrier reduction (see Supplementary Materials S2)

$$\Delta G = Lq\left[E_{water}^{normal} - E_{leak}/2\right], \tag{3}$$

with L taken as the total length of the molecule (comparable to the sensing region of our pores). Decreasing the thickness l of the Al_2O_3 leads to higher field leakage and lower fields inside the pore, reducing ΔG and leading to slower translocation events. For sufficiently long nanopores and small values of l, we may consider $E_{leak} = E_{water}^{normal}\left(\varepsilon_{film}/\varepsilon_{water}\right)$ and Eq. (3) can be simplified to $\Delta G = LqE_{leak}\left[\varepsilon_{water}/\varepsilon_{film} - 1/2\right]$. Estimating E_{leak} from Eq. (1), we find excellent quantitative agreement to translocation time data for dsDNA if we reduce the relative permittivity of water ε_{water} from 80 to 6 (see Fig. 6b). This adjustment is reasonable, as the dielectric constant of surficial water layer of two to three molecules thick is known to be significantly smaller than that of bulk water (the literature value is 2 to 20[60,61]) because the rotational freedom of water dipoles decreases for the immobile layers near the surface. Thus, the normal field leakage E_{leak} near the pore edge surface becomes higher than normally expected because of the weak screening effect of the immobile water layers. A water permittivity comparable to the dielectric film would indeed produce a leakage field that is comparable to the applied field, according to the thin-film limit of Eq. (1).

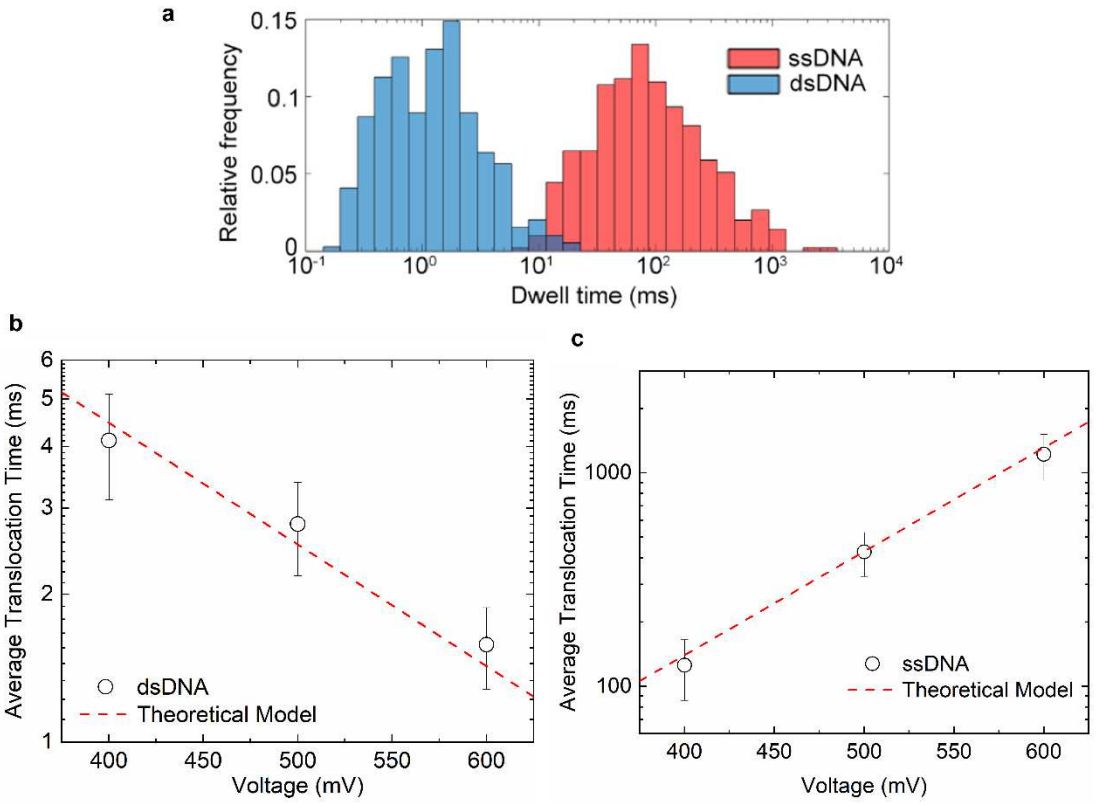

Figure 6. Comparison between dsDNA and ssDNA experimental translocation times. a, Normalized histogram of translocation times for 22nt ssDNA and 22bp dsDNA. ssDNA translocates much slower than dsDNA under the effect of electric field leakage (for a nanopore with a diameter of 10 nm, half cone angle ~ 7 ± 2° coated with 3 nm Al_2O_3 film under an applied voltage of 500 mV, typical translocation time ~ 1 ms (dsDNA) vs. ~ 100 ms (ssDNA)). These signature electrical signals allow discrimination (>97%) between ssDNA and dsDNA duplex translocation events (see Supplementary Materials S7). **b,** Average dsDNA translocation time dependence in function of the applied. The line represents the fit of the data to the model (Eq. (3) with $\tau_0 = 45$ ms, a charge per bp of 0.5e, and a length per bp of 0.34 nm[62]). **c,** Average ssDNA translocation time dependence in function of the applied. The line represents the fit of the data to the model (Eq. (4) with $\tau_0 = 1.595$ ms). **c,** Average ssDNA translocation time dependence in function of the applied. The line represents the fit of the data to the model (Eq. (4) with $\tau_0 = 1.595$ ms, a charge per nt of 0.1e, and a length per nt of 0.64 nm).

As $\varepsilon_{water}/\varepsilon_{film} > 1/2$, our previous derivation suggests that, even if all charges of a molecule see the same field leakage, translocation times should decrease exponentially with increasing voltage. We found an opposite trend for the 22 nt ssDNA (see Fig. 6c), whose translocation time increased exponentially with the applied voltage. This suggests that other than adjusting for the total number of charges *q*, (3) needs to be modified for ssDNA. Single stranded DNA molecules uncoil near hydrophobic surfaces, maximizing their hydrophobic interactions by means of increasing the contacts between the surface and their exposed aromatic rings[59]. In double stranded DNA molecules, this mechanism would require the breakage of the hydrogen bonds that stabilize the complementary base-pairs[63–65]. Therefore, hydrophobic interactions between double stranded DNA molecules and charged surfaces are limited to the two end base pairs, which have been suggested to present rapid (pico-seconds) opening and closing dynamics[66]. To cater to hydrophobic interactions present in ssDNA (and absent in their double stranded counterparts), a voltage-dependent term ΔG^* will be added to Eq. (3), which will model the van der Waals attraction of the hydrophobic rings of ssDNA towards the surface. We assume this term to be proportional to the field,

$$\Delta G^* = -\alpha L q E_{leak} \quad (4)$$

as field leakage brings the molecule into closer proximity to the membrane, stretching the molecule and thus increasing its affinity to the surface. Excellent agreement of our theory with experimental data is found by considering $\alpha \sim 0.9$ (see Fig. 6c), suggesting hydrophobic interactions amplifies electrostatic pinning of ssDNA molecules to the pore surface, to the extent that physical adsorption occurs. The additional term in (4) only applies to ssDNA.

This adsorption of ssDNA molecules to the pore surface is further confirmed by analyzing the current change associated to the translocation events. Due to their smaller cross-section area, single stranded molecules block less current than their double stranded counterparts, leading to lower current drops at high salt concentrations (such as the ones used in our experiments)[67,68] (see Fig. 7a). However, we observe comparable, if not higher, current drops for our single stranded molecule experiments (see Fig. 3 and 5), which can only result from significant modulation of the ionic conductivity due to surface effects[59]. In conic and bullet-shaped nanopores, the sensing area is localized near the tip, where the field is focused[50] and the surface charge of the thin alumina coating controls the ionic conductance in this key region. Adsorption of molecules near this region will then change the effective surface charge density of the pore walls (lowering it in our case, as Al_2O_3 is positively charged), depleting their counter-ions and leading to lower current. This would then lead to much higher current drops than for molecules translocating far from the pore walls[59] (see Fig. 7b). We have reproduced the resistive current pulses of 22-nt ssDNA and dsDNA of Fig. 2 by FEM simulation (Fig. 7), with comparable amplitudes for both due to adsorption of ssDNA.

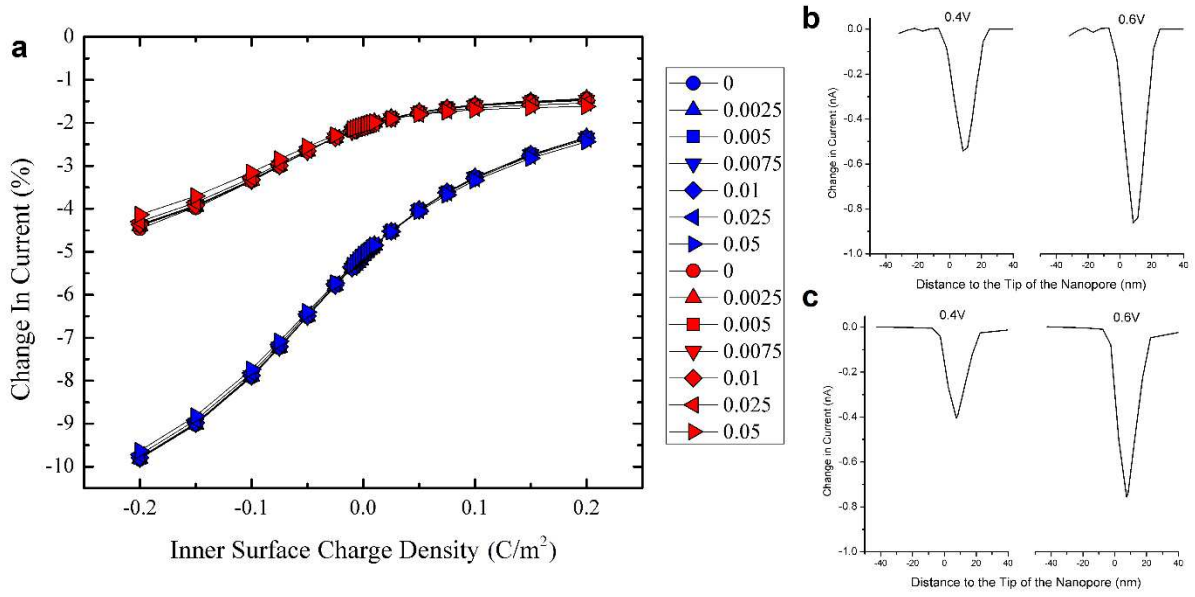

Figure 7. Finite-element-method simulation of the resistive signals. a, FEM simulated normalized change in current for a dsDNA molecule (blue) and a ssDNA molecule (red) translocating through the axis of a nanopore in function of the inner (horizontal axis) and outer (symbol shape) surface charge density at V_0=0.5V. Note that dsDNA molecules always leads to higher current drops than their single stranded counterparts, as they have higher cross-section areas. **b-d**, FEM simulated current drops for single stranded (b) and double stranded (c) molecules translocating through the walls and axis of the nanopore, respectively. Measurements taken at 0.4 (left) and 0.6 (right) V. Note that ssDNA molecules translocating through the pore walls present comparable resistive signals than their double stranded counterparts translocating through the bulk of the nanopore, in agreement with Fig. 3 and 5. Simulation details are presented in Supplementary Materials S3.

Finally, when the applied field is E_0 = 36.4 ± 6.1 V/μm, the average translocation time of ssDNA can be several minutes (Fig. 4a). Even under such strong normal leakage field, this electrostatic trapping effect is completely reversible.

This is illustrated in Fig. 8, where the current recovered to the base level after a negative applied voltage was applied. Once the direction of applied voltage and normal leakage field is reversed, the electrostatic trapping effect is switched off, and ssDNA can escape from the nanopore (see Supplementary Information S11). This reversible electrostatic trapping effect reduces the possibility of permanent nanopore blocking by translocating molecules, a common issue for nanopore sensors[69].

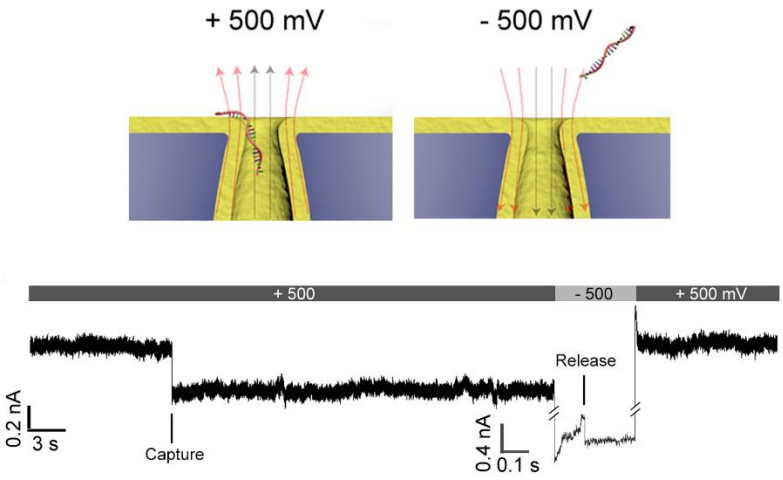

Figure 8. Reversibility of the molecular pinning. Electrical recording of 22 nt ssDNA pinning at the pore edge of a bullet-shaped Al_2O_3–coated (thickness, 3 nm) nanopores (diameter, 10 nm) with a half cone angles of 20 ± 3° under applied voltage of + 500 mV (energy barrier, 12.7 *kT*) and ssDNA escaping from the nanopore after the electrostatic trapping effect is switched off by reversing the polarity of applied voltage to – 500 mV.

Conclusions

We have designed a dielectric film coated solid-state nanopores in insulating polymer membranes, with an enhanced leakage field at the pore edge that can delay the translocation of ssDNA molecules by 5 orders of magnitude, thus providing a practical method to achieve up to 5 orders of temporal resolution enhancement for both sensing and sequencing applications. This large range of translocation times is due to an activated transport mechanism into the pore endowed by the pinning field, which can lead to actual adsorption, with an exponential dependence on the applied field and a barrier height that is sensitive to the affinity of the molecule to the surface. The prolonged molecular pinning time allows short nucleic acids to produce observable and distinct resistive signals and yet does not clog the nanopores or interfere with the resistive signal current. The reported enhanced sensitivity and selectivity would be useful for multiplex profiling of target microRNAs after hybridizing them with designed bar-coded oligos with dangling tails of different signature translocation times within the large range reported here. That the pinned ssDNA actually absorbs onto the edge suggests specific sequences or protein attachments can increase the library volume. Further studies of the interactions between DNA and normal field leakage in the context of voltage-driven DNA translocation may allow DNA translocate through the nanopore base by base, enabling a more controlled transport through nanopores equipped with transverse electrodes and allowing high-resolution sequencing or DNA/protein interaction analyses.

Methods

Fabrication of Al_2O_3-coated polymeric nanopore. The 12 μm thick polyethylene terephthalate (PET) foils were irradiated with single swift heavy ions (Au) with energy of 11.4 MeV per nucleon at the GSI in Darmstadt, Germany. An irradiated foil was subsequently etched at room temperature (295 K) by an asymmetric etching method, where the foil was mounted between two isolated containers that contained an etchant solution of 2.5 M NaOH in 1:1 MeOH/H2O and a stopping solution of 1 M HCOOH and 1 M KCl aqueous solution, respectively. The etching process started from one side of the PET foil, but was immediately stopped when etched through, and as a result, a single trumpet-like nanopore was formed on each irradiated PET foil. Bullet-shaped nanopores with different half cone angles were fabricated following an extended asymmetric etching procedure similar to that of Apel et al[51]. A secondary symmetric etching process (2M NaOH) was applied to enlarge the tip size. In all cases, the radius of the base was around 500 ± 80 nm, as determined by electron microscopy. The final tip radius was determined by an electrochemical method. Thermal ALD Al_2O_3 films of 3 or 10 nm were grown in a commercial (Cambridge Nanotech, Savannah S100) ALD reactor using trimethylaluminium (TMA) and de-ionized (DI) water as precursors. A low deposition temperature of 110 °C was chosen to prevent thermal damage to the polymer PET. Details on the fabrication of single asymmetric nanopores in polyethylene terephthalate (PET) membrane and subsequent deposition of Al_2O_3 dielectric films have been described previously[50].

.

Experiments of DNA Transport. A PET foil with a single Al_2O_3-coated polymeric nanopore was mounted between two isolated channels that were both filled with buffered 1 M KCl aqueous solution (0.01× PBS, pH = 7.4). A patch clamp amplifier (Axopatch 200B, Molecular Devices Inc.) with Ag/AgCl electrodes was used to measure the current trace and the current−voltage response across the nanopore. The polarity of the applied voltage was referenced to the tip side electrode. The current data were collected at 50 kHz with a low-pass Bessel filter of 10 kHz. For the DNA transport experiment, the buffered 10 pM 22 nt ssDNA and 22 bp dsDNA (Integrated DNA Technologies) solution (in 1 M KCl, 0.01× PBS, pH = 7.4) was always freshly made prior to each experiment and was injected to the tip side of the nanopore. 22bp dsDNA was obtained by hybridizing two complementary oligos and then purified by gel electrophoresis. Unless otherwise specified, a positive voltage of 500 mV was used in the transport experiment to drive the negatively charged molecules through the nanopore from tip to base.

Finite-Element-Method Simulations. All finite-element-method simulations were performed with the commercial code COMSOL. Simulation details of the field-leakage are presented in Supplementary Materials S1. Simulations of the translocation events were performed following a methodology previously published[59] and described in Supplementary Materials S3. 2D simulations were performed for the axisymmetric systems (bulk translocations) while 3D simulations were performed for the non-symmetric systems (adsorption). For each simulation, an initial mesh heavily refined on narrow regions, near the translocating agents, and near charged surfaces was considered. This mesh was refined through 5 mesh adaptation steps and convergence of the current was assessed during these adaptations (see Supplementary Materials S3).

Acknowledgements

The authors acknowledge support for this work from the National Institutes of Health (IMAT Grant No. R21CA206904). The authors acknowledge that ZP was supported by a China Scholarship Council fellowship. We are grateful to C. Trautmann, J.M. Xue and Y.G. Wang for providing the irradiated PET membrane samples.

Bibliography

1. Venkatesan, B. M. & Bashir, R. Nanopore sensors for nucleic acid analysis. *Nature Nanotechnology* **6**, 615–624 (2011).
2. Wanunu, M. Nanopores: A journey towards DNA sequencing. *Physics of Life Reviews* **9**, 125–158 (2012).
3. Deamer, D., Akeson, M. & Branton, D. Three decades of nanopore sequencing. *Nature Biotechnology* **34**, 518–524 (2016).
4. Yusko, E. C. *et al.* Controlling protein translocation through nanopores with bio-inspired fluid walls. *Nature Nanotechnology* **6**, 253–260 (2011).
5. Kennedy, E., Dong, Z., Tennant, C. & Timp, G. Reading the primary structure of a protein with 0.07 nm 3 resolution using a subnanometre-diameter pore. *Nature Nanotechnology* **11**, 968–976 (2016).
6. Smeets, R. M. M., Kowalczyk, S. W., Hall, A. R., Dekker, N. H. & Dekker, C. Translocation of RecA-Coated Double-Stranded DNA through Solid-State Nanopores. *Nano Lett.* **9**, 3089–3095 (2009).
7. Dekker, C. Solid-state nanopores. *Nature Nanotechnology* **2**, 209–215 (2007).
8. Branton, D. *et al.* The potential and challenges of nanopore sequencing. *Nat. Biotechnol.* **26**, 1146–1153 (2008).
9. Di Ventra, M. & Taniguchi, M. Decoding DNA, RNA and peptides with quantum tunnelling. *Nature Nanotechnology* **11**, 117–126 (2016).
10. Fologea, D., Uplinger, J., Thomas, B., McNabb, D. S. & Li, J. Slowing DNA Translocation in a Solid-State Nanopore. *Nano Lett.* **5**, 1734–1737 (2005).
11. Meller, A., Nivon, L. & Branton, D. Voltage-driven DNA translocations through a nanopore. *Phys. Rev. Lett.* **86**, 3435–3438 (2001).
12. Muthukumar, M. Mechanism of DNA Transport Through Pores. *Annual Review of Biophysics and Biomolecular Structure* **36**, 435–450 (2007).
13. Plesa, C. *et al.* Fast Translocation of Proteins through Solid State Nanopores. *Nano Lett.* **13**, 658–663 (2013).
14. Rosenstein, J. K., Wanunu, M., Merchant, C. A., Drndic, M. & Shepard, K. L. Integrated nanopore sensing platform with sub-microsecond temporal resolution. *Nature Methods* **9**, 487–492 (2012).
15. Venta, K. *et al.* Differentiation of Short, Single-Stranded DNA Homopolymers in Solid-State Nanopores. *ACS Nano* **7**, 4629–4636 (2013).
16. Smeets, R. M. M., Keyser, U. F., Dekker, N. H. & Dekker, C. Noise in solid-state nanopores. *Proc. Natl. Acad. Sci. U.S.A.* **105**, 417–421 (2008).
17. Wanunu, M. *et al.* Rapid electronic detection of probe-specific microRNAs using thin nanopore sensors. *Nat Nanotechnol* **5**, 807–814 (2010).
18. Wang, Y., Zheng, D., Tan, Q., Wang, M. & Gu, L.-Q. Nanopore-based detection of circulating microRNAs in lung cancer patients. *Nat Nanotechnol* **6**, 668–674 (2011).
19. Yokota, K., Tsutsui, M. & Taniguchi, M. Electrode-embedded nanopores for label-free single-molecule sequencing by electric currents. *RSC Adv.* **4**, 15886–15899 (2014).
20. Yuan, Z., Liu, Y., Dai, M., Yi, X. & Wang, C. Controlling DNA Translocation Through Solid-state Nanopores. *Nanoscale Research Letters* **15**, 80 (2020).
21. Kowalczyk, S. W., Wells, D. B., Aksimentiev, A. & Dekker, C. Slowing down DNA Translocation through a Nanopore in Lithium Chloride. *Nano Lett.* **12**, 1038–1044 (2012).
22. Yeh, L.-H., Zhang, M., Joo, S. W. & Qian, S. Slowing down DNA translocation through a nanopore by lowering fluid temperature. *Electrophoresis* **33**, 3458–3465 (2012).
23. Luan, B. *et al.* Base-by-base ratcheting of single stranded DNA through a solid-state nanopore. *Phys. Rev. Lett.* **104**, 238103 (2010).
24. Verschueren, D. V. *et al.* Label-Free Optical Detection of DNA Translocations through Plasmonic Nanopores. *ACS Nano* **13**, 61–70 (2019).
25. Hall, A. R. *et al.* Hybrid pore formation by directed insertion of alpha hemolysin into solid-state nanopores. *Nat Nanotechnol* **5**, 874–877 (2010).
26. Cherf, G. M. *et al.* Automated forward and reverse ratcheting of DNA in a nanopore at 5-Å precision. *Nat. Biotechnol.* **30**, 344–348 (2012).
27. Manrao, E. *et al.* Reading DNA at a Single-Nucleotide Resolution with a Mutant MspA nanopore and phi29 DNA Polymerase. *Nature biotechnology* **30**, 349–53 (2012).
28. Nam, S.-W., Rooks, M. J., Kim, K.-B. & Rossnagel, S. M. Ionic Field Effect Transistors with Sub-10 nm Multiple Nanopores. *Nano Lett.* **9**, 2044–2048 (2009).
29. Banerjee, S. *et al.* Slowing DNA Transport Using Graphene-DNA Interactions. *Adv Funct Mater* **25**, 936–946 (2015).
30. Larkin, J. *et al.* Slow DNA Transport through Nanopores in Hafnium Oxide Membranes. *ACS Nano* **7**, 10121–10128 (2013).
31. Jiang, Z. & Stein, D. Charge regulation in nanopore ionic field-effect transistors. *Phys. Rev. E* **83**, 031203 (2011).
32. Venkatesan, B. M. *et al.* Stacked Graphene-Al2O3 Nanopore Sensors for Sensitive Detection of DNA and DNA–Protein Complexes. *ACS Nano* **6**, 441–450 (2012).
33. Di Fiori, N. *et al.* Optoelectronic control of surface charge and translocation dynamics in solid-state nanopores. *Nature Nanotechnology* **8**, 946–951 (2013).

34. Miles, B. N. *et al.* Single molecule sensing with solid-state nanopores: novel materials, methods, and applications. *Chem. Soc. Rev.* **42**, 15–28 (2012).
35. Venkatesan, B. M., Shah, A. B., Zuo, J.-M. & Bashir, R. DNA Sensing Using Nanocrystalline Surface-Enhanced Al2O3 Nanopore Sensors. *Advanced Functional Materials* **20**, 1266–1275 (2010).
36. Murarka, S. P. Silicon Dioxide, Nitride, and Oxynitride. in *Encyclopedia of Materials: Science and Technology* (eds. Buschow, K. H. J. et al.) 1–14 (Elsevier, 2003). doi:10.1016/B0-08-043152-6/01895-7.
37. Pedroli, F. *et al.* Reducing leakage current and dielectric losses of electroactive polymers through electro-annealing for high-voltage actuation. *RSC Advances* **9**, 12823–12835 (2019).
38. Schroeder, H. & Schmitz, S. Thickness dependence of leakage currents in high-permittivity thin films. *Appl. Phys. Lett.* **83**, 4381–4383 (2003).
39. Sarma, K. C. D. & Sharma, S. A method for reduction of off state leakage current in symmetric DG JLT. *Eng. Res. Express* **1**, 015034 (2019).
40. Atanassova, E. & Dimitrova, T. Chapter 9 - THIN Ta2O5 LAYERS ON Si AS AN ALTERNATIVE TO SiO2 FOR HIGH-DENSITY DRAM APPLICATIONS. in *Handbook of Surfaces and Interfaces of Materials* (ed. Nalwa, H. S.) 439–479 (Academic Press, 2001). doi:10.1016/B978-012513910-6/50055-4.
41. Lin, H. C., Ye, P. D. & Wilk, G. D. Leakage current and breakdown electric-field studies on ultrathin atomic-layer-deposited Al2O3 on GaAs. *Appl. Phys. Lett.* **87**, 182904 (2005).
42. Thamida, S. K. & Chang, H.-C. Nonlinear electrokinetic ejection and entrainment due to polarization at nearly insulated wedges. *Physics of Fluids* **14**, 4315–4328 (2002).
43. Eckstein, Y., Yossifon, G., Seifert, A. & Miloh, T. Nonlinear electrokinetic phenomena around nearly insulated sharp tips in microflows. *J Colloid Interface Sci* **338**, 243–249 (2009).
44. Gramotnev, D. K. & Bozhevolnyi, S. I. Nanofocusing of electromagnetic radiation. *Nature Photonics* **8**, 13–22 (2014).
45. Deygout, J. Multiple knife-edge diffraction of microwaves. *IEEE Transactions on Antennas and Propagation* **14**, 480–489 (1966).
46. Collins, R. T., Sambath, K., Harris, M. T. & Basaran, O. A. Universal scaling laws for the disintegration of electrified drops. *Proc. Natl. Acad. Sci. U.S.A.* **110**, 4905–4910 (2013).
47. Tabard-Cossa, V., Trivedi, D., Wiggin, M., Jetha, N. N. & Marziali, A. Noise analysis and reduction in solid-state nanopores. *Nanotechnology* **18**, 305505 (2007).
48. Lee, M.-H. *et al.* A Low-Noise Solid-State Nanopore Platform Based on a Highly Insulating Substrate. *Scientific Reports* **4**, 7448 (2014).
49. Apel, P. Y., Korchev, Yu. E., Siwy, Z., Spohr, R. & Yoshida, M. Diode-like single-ion track membrane prepared by electro-stopping. *Nuclear Instruments and Methods in Physics Research Section B: Beam Interactions with Materials and Atoms* **184**, 337–346 (2001).
50. Wang, C. *et al.* Atomic Layer Deposition Modified Track-Etched Conical Nanochannels for Protein Sensing. *Anal. Chem.* **87**, 8227–8233 (2015).
51. Py, A. *et al.* Shedding light on the mechanism of asymmetric track etching: an interplay between latent track structure, etchant diffusion and osmotic flow. *Phys Chem Chem Phys* **18**, 25421–25433 (2016).
52. Wu, L. *et al.* Electrically facilitated translocation of protein through solid nanopore. *Nanoscale Res Lett* **9**, 140 (2014).
53. Liu, Q. *et al.* Voltage-Driven Translocation of DNA through a High Throughput Conical Solid-State Nanopore. *PLOS ONE* **7**, e46014 (2012).
54. Zhang, J. & Shklovskii, B. I. Effective charge and free energy of DNA inside an ion channel. *Phys. Rev. E* **75**, 021906 (2007).
55. Wanunu, M., Sutin, J., McNally, B., Chow, A. & Meller, A. DNA Translocation Governed by Interactions with Solid-State Nanopores. *Biophys J* **95**, 4716–4725 (2008).
56. Ghosal, S., Sherwood, J. D. & Chang, H.-C. Solid-state nanopore hydrodynamics and transport. *Biomicrofluidics* **13**, 011301 (2019).
57. Chang, H. & Yeo, L. *Electrokinetically driven microfluidics and nanofluidics*. (Cambridge University Press, 2010).
58. Ghosal, S. Electrophoresis of a polyelectrolyte through a nanopore. *Phys Rev E Stat Nonlin Soft Matter Phys* **74**, 041901 (2006).
59. Sensale, S., Wang, C. & Chang, H.-C. Resistive Amplitude Fingerprints during Translocation of Linear MoleculesThrough Charged Solid-State Nanopores. *J. Chem. Phys.* **153**, 085102 (2020).
60. Fumagalli, L. *et al.* Anomalously low dielectric constant of confined water. *Science* **360**, 1339–1342 (2018).
61. Cherepanov, D. A., Feniouk, B. A., Junge, W. & Mulkidjanian, A. Y. Low dielectric permittivity of water at the membrane interface: effect on the energy coupling mechanism in biological membranes. *Biophys. J.* **85**, 1307–1316 (2003).
62. Sensale, S., Peng, Z. & Chang, H.-C. Biphasic signals during nanopore translocation of DNA and nanoparticles due to strong ion cloud deformation. *Nanoscale* **11**, 22772–22779 (2019).
63. Kwon, K. D., Vadillo-Rodriguez, V., Logan, B. E. & Kubicki, J. D. Interactions of biopolymers with silica surfaces: Force measurements and electronic structure calculation studies. *Geochimica et Cosmochimica Acta* **70**, 3803–3819 (2006).

64. Isailovic, S., Li, H.-W. & Yeung, E. S. Adsorption of single DNA molecules at the water/fused-silica interface. *Journal of Chromatography A* **1150**, 259–266 (2007).
65. Shi, B., Shin, Y. K., Hassanali, A. A. & Singer, S. J. DNA Binding to the Silica Surface. *J. Phys. Chem. B* **119**, 11030–11040 (2015).
66. Andreatta, D. *et al.* Ultrafast Dynamics in DNA: "Fraying" at the End of the Helix. *J Am Chem Soc* **128**, 6885–6892 (2006).
67. Smeets, R. M. M. *et al.* Salt Dependence of Ion Transport and DNA Translocation through Solid-State Nanopores. *Nano Lett.* **6**, 89–95 (2006).
68. Skinner, G. M., van den Hout, M., Broekmans, O., Dekker, C. & Dekker, N. H. Distinguishing single- and double-stranded nucleic acid molecules using solid-state nanopores. *Nano Lett.* **9**, 2953–2960 (2009).
69. Agah, S., Zheng, M., Pasquali, M. & Kolomeisky, A. B. DNA sequencing by nanopores: advances and challenges. *J. Phys. D: Appl. Phys.* **49**, 413001 (2016).

Figures

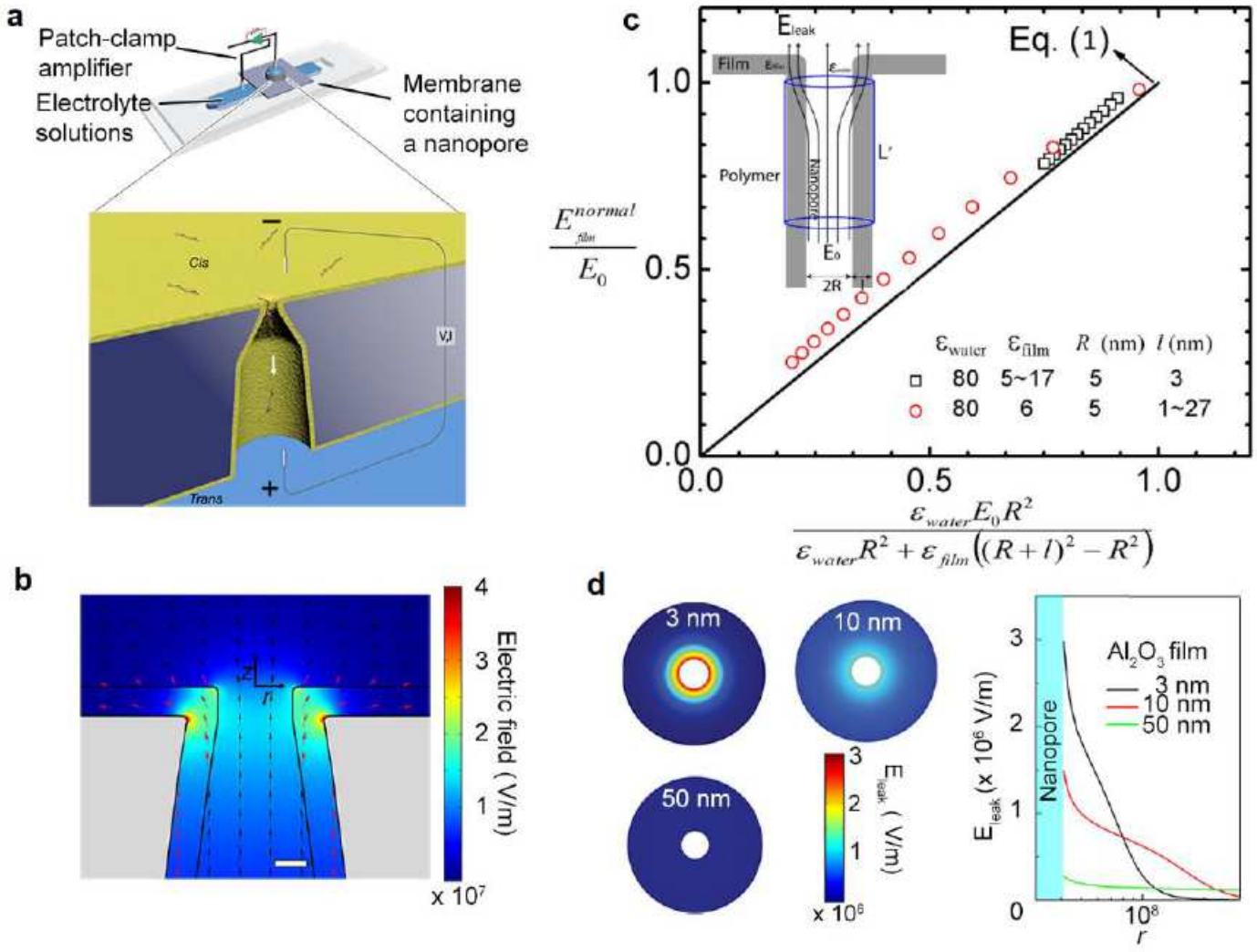

Figure 1

The electric field leakage effect in Al2O3-coated polymer nanopores. a. Set-up to measure resistive pulses from the translocation of individual DNA molecules through single bullet-shaped polymer nanopore coated with a thin Al2O3 layer. b. Electrostatic modelling of a Al2O3-coated bullet-like nanopore (tip diameter: 8 nm, half cone angle: 8o) was simulated with an applied voltage of 0.5 V. Electric field lines and intensity evaluated numerically on the tip side of the Al2O3-coated polymer nanopore. The electric field is significantly enhanced and develops a normal field leakage near the sharp pore edge. Scale bar = 3 nm. c. Validation of Eq. (1) through the use of finite-element-method simulations for normal field leakage in the dielectric film. Different permittivities and film thicknesses were sampled. Inset shows the schematics of a high-permittivity dielectric film on an insulating polymer nanopore orifice and the Gauss volume used to estimate the leaked field around the pore. d. Left: Surface plots of the strength of normal leakage field (Eleak) showing the normal leakage field at the pore edge is a strong function of Al2O3 film

thickness (nanopore diameter, 8 nm). Right: Axial dependence of the normal leakage field as a function of distance from the pore mouth r for three Al2O3 film thicknesses.

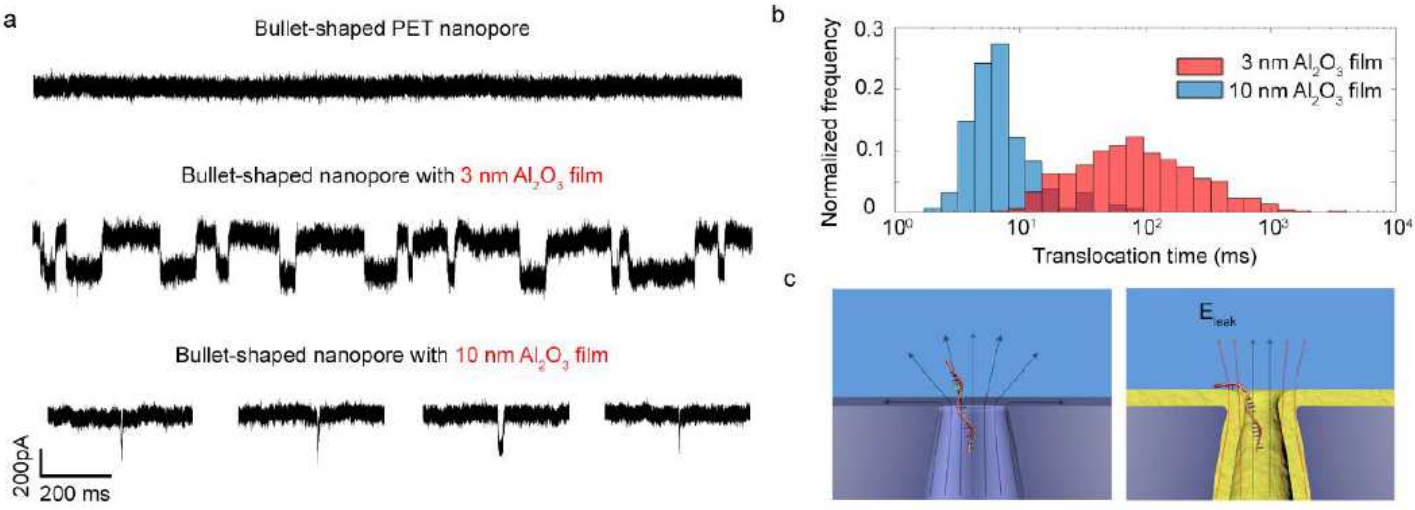

Figure 2

Slowing down ssDNA translocation speed with electric field leakage. a, Representative current traces for 22 nt ssDNA translocation through a bare bullet-shaped PET nanopore without Al2O3 film coating (diameter, 16 nm) and two bullet-shaped nanopores coated with 3 nm or 10 nm Al2O3 film under an applied voltage of 500 mV. Both Al2O3-coated nanopores have the same final tip diameter (10 nm). All three nanopores have similar bullet-like shapes (half cone angle ~ 7 ± 2o). Slow translocation of 22 nt ssDNA is observed using nanopores with thin Al2O3 film coating and the average translocation time is a function of film thickness. b, Normalized histogram of translocation times for nanopores with 3 nm or 10 nm Al2O3 film. Average translocation time: 3 nm Al2O3 film, 159 ms; 10 nm, 13 ms. c, Schematic showing the dominant tangential electric field at the bare PET nanopore edge results in a fast translocation of 22 nt ssDNA (left) while the normal leakage field at the Al2O3-coated nanopore edge traps the ssDNA and thus reduces its mobility.

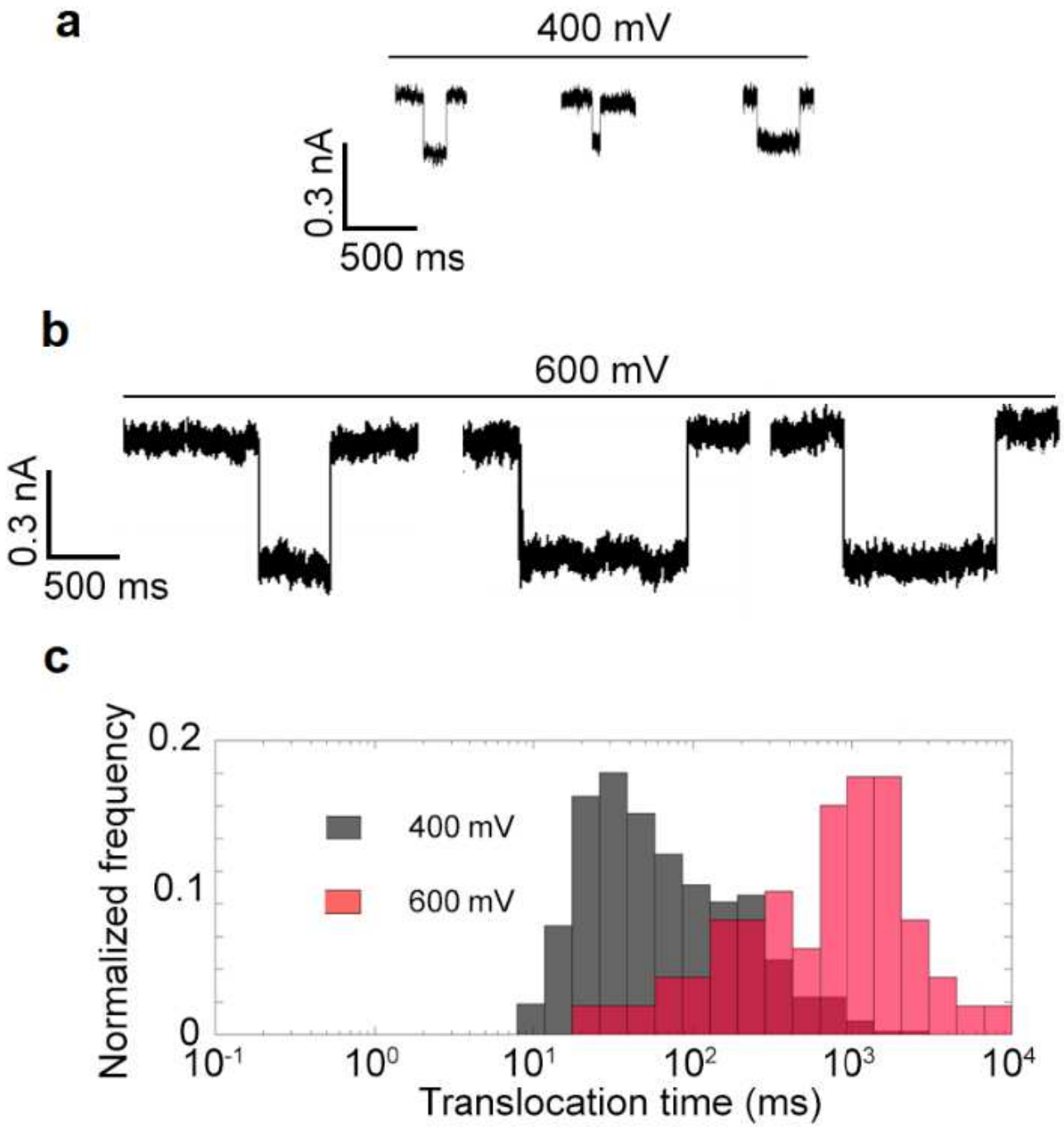

Figure 3

Effects of electric field leakage on ssDNA transport. a, Representative translocation signals for 22 nt ssDNA translocations at applied voltages of 400 mV. b, Representative translocation signals for 22 nt ssDNA translocations at applied voltages of 600 mV. c, Normalized histogram of corresponding translocation times at applied voltages of 400 mV and 600 mV and average translocation time as a function of applied voltage. Increasing the strength of electric field leakage can increase the translocation time of ssDNA. Data were acquired using a nanopore coated with 3 nm Al2O3 film (diameter, 8 nm; half cone angle, 9 ± 2o).

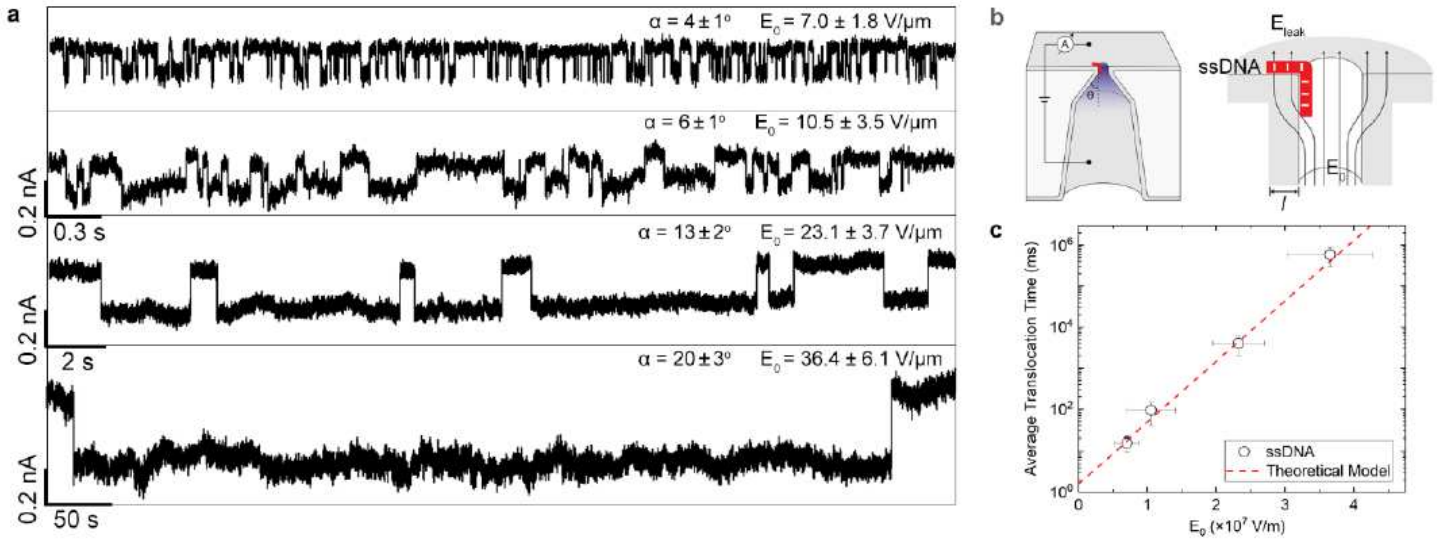

Figure 4

Modulation of translocation dynamics by angle control. a, Representative current traces of 22 nt ssDNA translocating through four bullet-shaped Al2O3–coated (thickness, 3 nm) nanopores (diameter, 10 nm) with different half cone angles (α). The nanopores with larger cone angle allow more electric field (E0, as indicated) to be focused at the nanopore tip under the same applied voltage (500 mV) and thus higher magnitude of normal leakage field at the pore edge. With the increase of half cone angle and thus normal leakage field, the average translocation time can be increased exponentially from milliseconds to hundreds of seconds. b, Left: schematic of the measurement apparatus using a bullet-shaped Al2O3–coated nanopores with a half cone angles of θ. Right: zoom in of the nanopore orifice with ssDNA electrostatically trapped at the pore edge by the normal leakage field. c, The average translocation time dependence of E0. The line represents the fit of the data to the theoretical model Eq. (4) with 0=1.595 ms, a charge per nt of 0.1e, and a length per nucleotide of 0.64nm59.

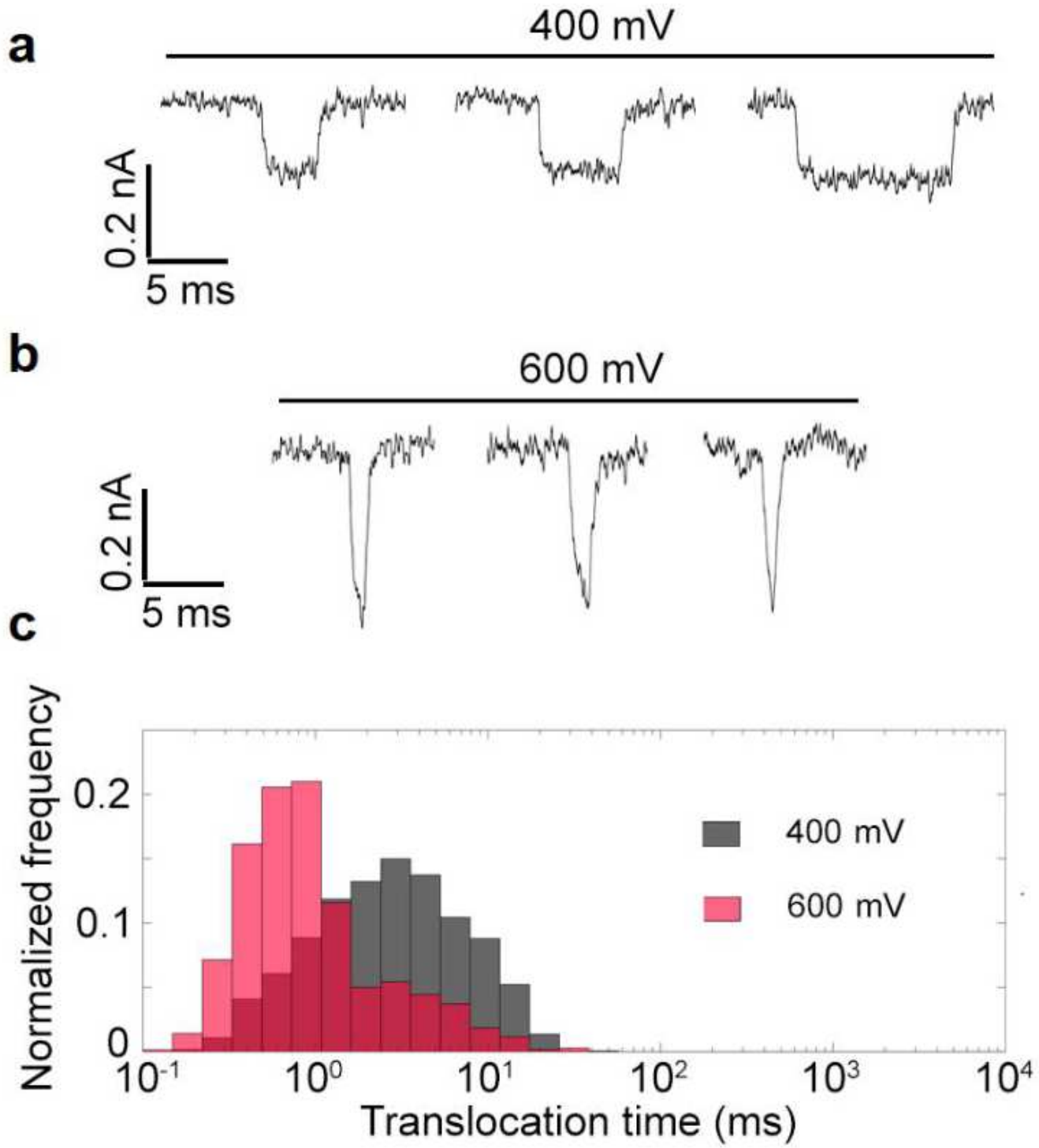

Figure 5

Effects of electric field leakage on dsDNA transport. a, Rrepresentative translocation signals for 22 bp dsDNA translocations at applied voltages of 400 mV. b, Rrepresentative translocation signals for 22 bp dsDNA translocations at applied voltages of 600 mV. c, Normalized histogram of corresponding translocation times at applied voltages of 400 mV and 600 mV and average translocation time as a function of applied voltage. Increasing the strength of electric field leakage decreases the translocation

time of dsDNA. Data were acquired using a nanopore coated with 3 nm Al2O3 film (diameter, 8 nm; half cone angle, 9 ± 2o).

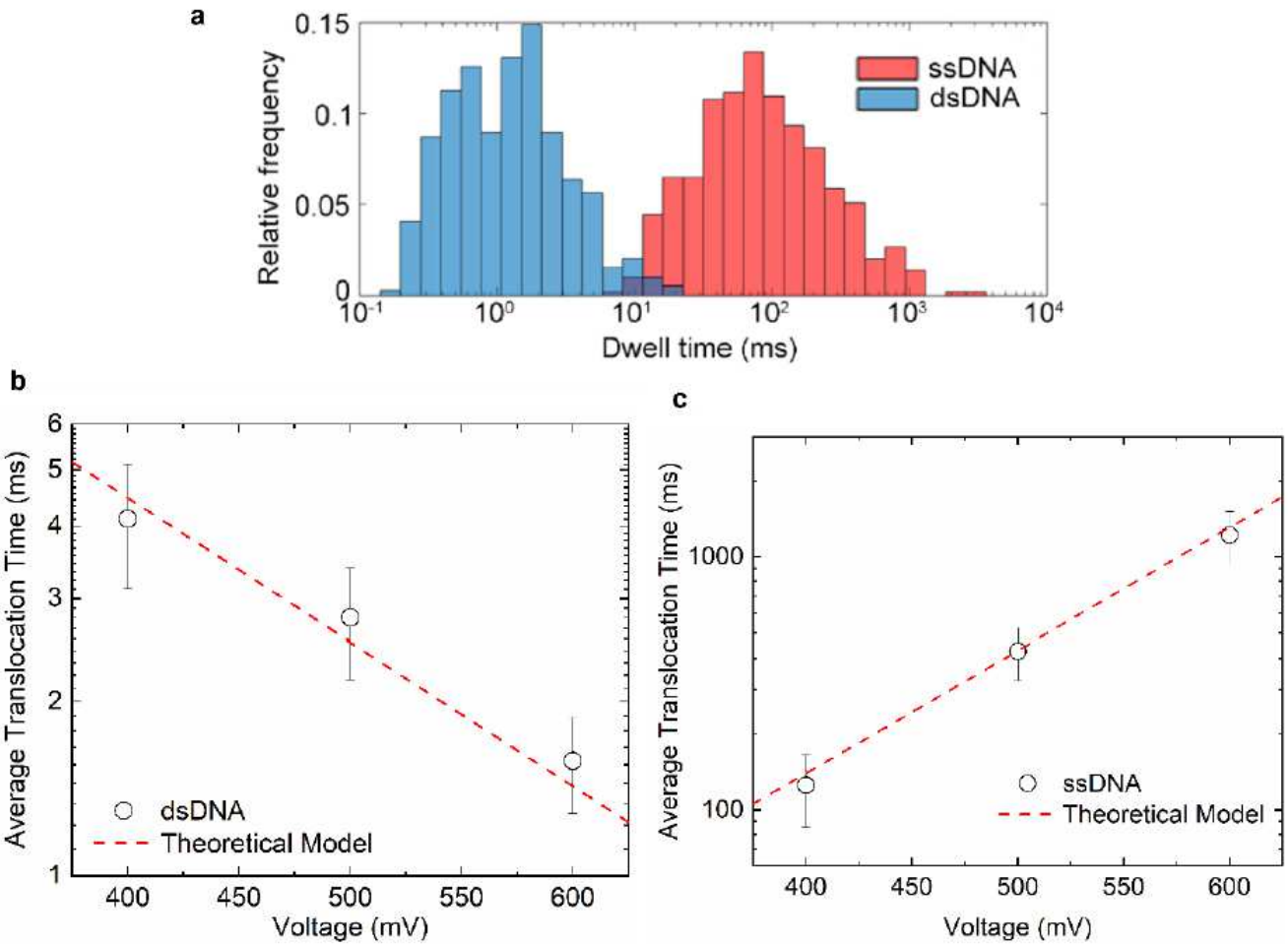

Figure 6

Comparison between dsDNA and ssDNA experimental translocation times. a, Normalized histogram of translocation times for 22nt ssDNA and 22bp dsDNA. ssDNA translocates much slower than dsDNA under the effect of electric field leakage (for a nanopore with a diameter of 10 nm, half cone angle ~ 7 ± 2o coated with 3 nm Al2O3 film under an applied voltage of 500 mV, typical translocation time ~ 1 ms (dsDNA) vs. ~ 100 ms (ssDNA)). These signature electrical signals allow discrimination (>97%) between ssDNA and dsDNA duplex translocation events (see Supplementary Materials S7). b, Average dsDNA translocation time dependence in function of the applied. The line represents the fit of the data to the model (Eq. (3) with 0=45 ms, a charge per bp of 0.5e, and a length per bp of 0.34 nm62). c, Average ssDNA translocation time dependence in function of the applied. The line represents the fit of the data to the model (Eq. (4) with 0=1.595 ms). c, Average ssDNA translocation time dependence in function of the applied. The line represents the fit of the data to the model (Eq. (4) with 0=1.595 ms, a charge per nt of 0.1e, and a length per nt of 0.64 nm).

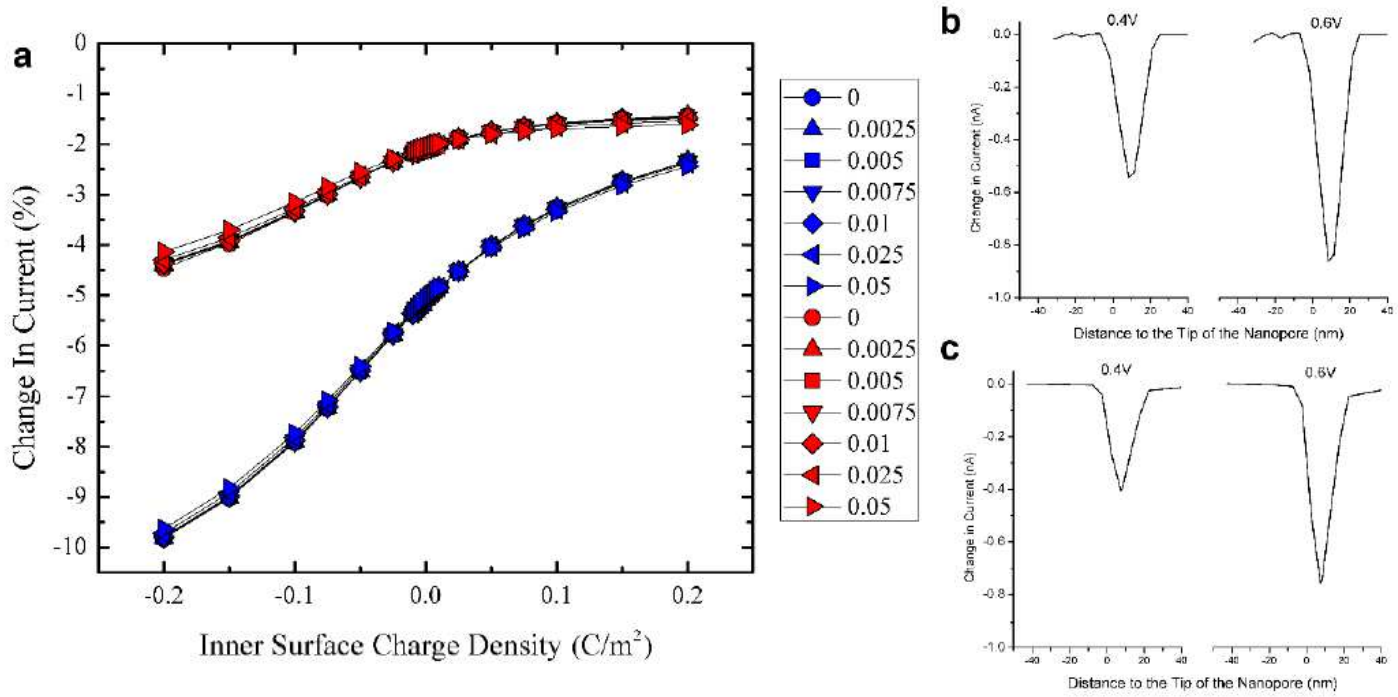

Figure 7

Finite-element-method simulation of the resistive signals. a, FEM simulated normalized change in current for a dsDNA molecule (blue) and a ssDNA molecule (red) translocating through the axis of a nanopore in function of the inner (horizontal axis) and outer (symbol shape) surface charge density at V0=0.5V. Note that dsDNA molecules always leads to higher current drops than their single stranded counterparts, as they have higher cross-section areas. b-d, FEM simulated current drops for single stranded (b) and double stranded (c) molecules translocating through the walls and axis of the nanopore, respectively. Measurements taken at 0.4 (left) and 0.6 (right) V. Note that ssDNA molecules translocating through the pore walls present comparable resistive signals than their double stranded counterparts translocating through the bulk of the nanopore, in agreement with Fig. 3 and 5. Simulation details are presented in Supplementary Materials S3.

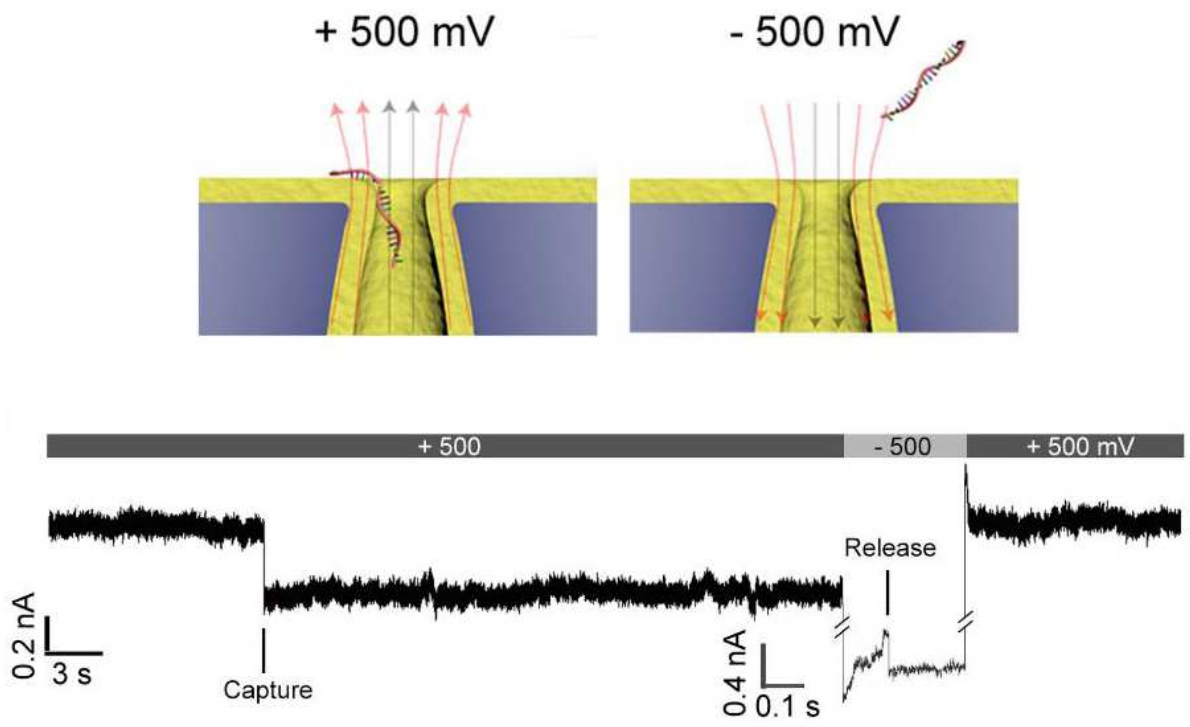

Figure 8

Reversibility of the molecular pinning. Electrical recording of 22 nt ssDNA pinning at the pore edge of a bullet-shaped Al2O3–coated (thickness, 3 nm) nanopores (diameter, 10 nm) with a half cone angles of 20 ± 3o under applied voltage of + 500 mV (energy barrier, 12.7 kT) and ssDNA escaping from the nanopore after the electrostatic trapping effect is switched off by reversing the polarity of applied voltage to – 500 mV.

Supplementary Files

This is a list of supplementary files associated with this preprint. Click to download.

- SupplementaryMaterials.pdf